Spin-lattice-coupling-mediated magnetoferroelectric phase transition induced by uniaxial pressure in multiferroic $CuFe_{1-x}M_xO_2$ (M = Ga, Al)

Hiromu Tamatsukuri,* Setsuo Mitsuda, Tenfu Nakamura, Kouhei Takata, and Taro Nakajima†

Department of Physics, Faculty of Science, Tokyo University of Science, Tokyo 162-8601, Japan

Karel Prokes, Fabiano Yokaichiya, and Klaus Kiefer

Helmholtz-Zentrum Berlin for Materials and Energy, Hahn-Meitner-Platz 1, Berlin 14109, Germany

(Dated: May 14, 2017)

Abstract

We have investigated magnetic and ferroelectric (dielectric) properties of multiferroic $CuFe_{0.982}Ga_{0.018}O_2$, $CuFe_{0.965}Ga_{0.035}O_2$ and $CuFe_{0.95}Al_{0.05}O_2$ under applied uniaxial pressure p up to 600 MPa. Unlike the results of the almost same experiments on $CuFeO_2$ [Tamatsukuri *et al.* Phys. Rev. B **94** 174402 (2016)], we have found that the application of p induces a new ferroelectric phase, which is different from the well-studied spin-driven ferroelectric phase with helical magnetic ordering, in all the doped samples investigated here. We have also constructed the temperature versus p magnetoelectric phase diagrams of the three samples. The ferroelectric polarization in the p-induced ferroelectric phase lies along the [110] direction as in the helical magneto-ferroelectric phase, and its value is comparable with or larger than that in the helical magneto-ferroelectric phase. The magnetic structure in the p-induced ferroelectric phase seems to be of a collinear sinusoidal type. Although this magnetic structure itself does not break the inversion symmetry, it is considered to play an important role in the origin of ferroelectricity in the p-induced ferroelectric phase through the spin-lattice coupling in this system.

PACS numbers: 75.85.+t, 75.80.+q, 77.80.-e, 75.50.Ee

I. INTRODUCTION

Since the discovery of magnetic control of ferroelectric polarization in $TbMnO_3$, spin-driven ferroelectricity has attracted great interest in condensed matter physics[1–3]. One of key factors governing the emergence of the spin-driven ferroelectricity is complex spin texture breaking inversion symmetry in the systems. Owing to a tendency to exhibit such a magnetic structure, geometrically frustrated magnets have been recognized as one of the candidates for the spin-driven ferroelectric materials. Following this strategy, many spin-driven ferroelectric materials have been found during the past decade[4,5]. On the other hand, several frustrated magnets are often spin-lattice coupled systems, in which magnetic phase transitions are accompanied by spontaneous lattice distortions that partially relieve the frustration between spins[6–9]. As a result, spin-driven ferroelectric materials with a spin-lattice coupling offer a possibility that novel magnetoelectric effects can be realized by the application of anisotropic pressure conjugating to spontaneous lattice distortions. In this paper, we demonstrate that in multiferroic $CuFe_{1-x}M_xO_2$ (M = Ga, Al), the application of uniaxial pressure induces a new ferroelectric phase transition, which would be mediated by the spin-lattice coupling.

Our target materials, $CuFe_{1-x}M_xO_2$ (M = Ga, Al) (abbreviated as CFGO and CFAO, hereafter), have both of the spin-driven ferroelectricity and the strong spin-lattice coupling. The delafossite $CuFeO_2$ is known as a typical example of triangular-lattice antiferromagnets with the geometrical frustration, in which the magnetic moment is carried by Fe^{3+} ion ($S = 5/2$)[10,11]. Because of the frustration, the substitution of a few percent of nonmagnetic M^{3+} for Fe^{3+} causes a rich x-temprature (T) phase diagram, as shown in Figs. 1 (a) and 1 (b)[12]. For example, CFGO with x = 0.035 undergoes three successive magnetic transitions[13]: a paramagnetic (PM) phase ($T \geq T_{\rm N1} = 14$ K) $\rightarrow$ a oblique partially disordered (OPD) phase ($T_{\rm N2}^{\rm high} \simeq 10$ K $\leq T \leq T_{\rm N1}$) $\rightarrow$ a partially disordered (PD) phase ($T_{\rm N2}^{\rm low} \simeq 7$ K $\leq T \leq T_{\rm N2}^{\rm high}$) $\rightarrow$ a ferroelectric incommensurate magnetic (FE-ICM) phase ($T \leq T_{\rm N2}^{\rm low}$). In the PD and the OPD phases, collinear sinusoidal magnetic ordering with a magnetic modulation wave vector (q,q,3/2) is realized[11,14]. The magnetic moments are oriented to the c axis and q is dependent on T [q = 0.197-0.207] in the PD phase, while the sinusoidal ordering in the OPD phase is oblique from the c axis by $\sim 50^\circ$ with T invariant $q \simeq 0.194$. The FE-ICM phase has a screw helical magnetic structure with a locked wave vector (q,q,3/2; $q \simeq 0.202$),

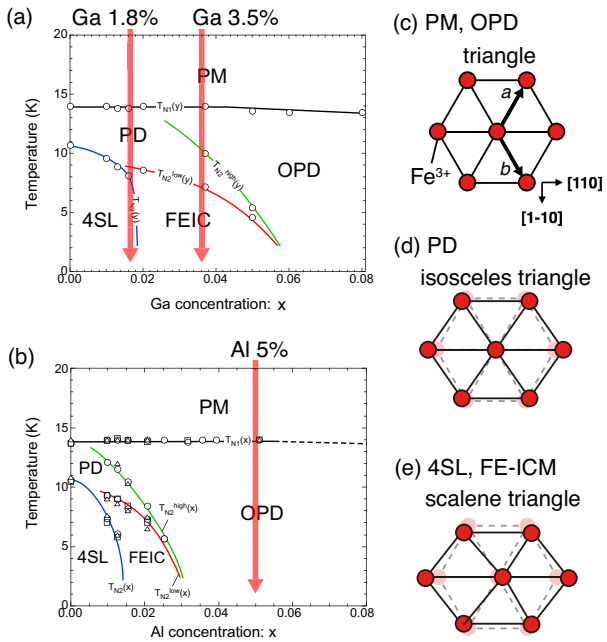

FIG. 1. (Color Online) x-T magnetic phase diagram of $CuFe_{1-x}M_xO_2$ for (a) M = Ga and for (b) M = Al. The diagrams are taken from Ref. 12. [(c)-(e)] Schematics of Fe^{3+} triangular lattice in (c) the PM and the OPD phases, (d) the PD phase, and (e) the FE-ICM phase.

whose screw axis is parallel to the [110] direction[15]. The FE-ICM phase exhibits the spin-driven ferroelectricity: the helical magnetic structure induces a ferroelectric polarization (P) $\parallel$ [110] through the Fe3d-O2p hybridization mechanism, where there is a one-to-one correspondence between the direction of P and the helicity (left-handed or right-handed helical arrangement of spins)[16,17]. In addition to these phases, a collinear 4SL phase, in which the magnetic moments are collinearly arranged ($\uparrow\uparrow\downarrow\downarrow$) along c axis with the magnetic modulation vector (1/4,1/4,3/2), is realized in the low-x regions.

These magnetic phase transitions are accompanied by spontaneous monoclinic lattice distortions, except for the transition from the PM phase to the OPD phase[18–20]. Previous synchrotron radiation x-ray diffraction studies revealed triangular lattices in each magnetic phase, as shown in Figs. 1 (c) – 1 (e)[21]. During the deformation, the crystal axes elongate along the [110] direction and contract along the [1$\bar{1}$0] direction. Therefore, the application of an uniaxial pressure p along the [1$\bar{1}$0] direction supports the spontaneous lattice distortion in this system.

Quite recently, we developed a technique that enables the application of p up to 600 MPa

for $CuFeO_2$[22]. In this study, we have systematically investigated the magnetic and ferroelectric (dielectric) properties of CFGO with x = 0.035, 0.018 and CFAO with x = 0.050 under applied p along the $[1\bar{1}0]$ direction up to 600 MPa. These samples show the characteristic phase transitions from the viewpoint of the lattice distortion and the ferroelectricity; as shown in Figs. 1 (a) and 1 (b), the Ga 3.5% and Ga 1.8% samples exhibit the spin-driven ferroelectric FE-ICM phase as the ground state and as the thermally intermediate state, respectively; and the OPD phase, in which the spontaneous lattice distortion does not occur, shows up as the thermally intermediate state and as the ground state in Ga 3.5% and in Al 5.0% samples, respectively. Unlike the results of $CuFeO_2$ (x = 0.00)[22], applied p induces a new ferroelectric phase that differs from the FE-ICM phase in all the doped samples investigated here. The magnetic structure in the p-induced ferroelectric phase seems to be of the collinear sinusoidal type, which alone dose not break the inversion symmetry. Nevertheless, the magnetic structure is considered to play a important role in the origin of ferroelectricity in the p-induced ferroelectric phase through the spin-lattice coupling. Based on these experimental results, we discuss the possible origin of ferroelectricity in the p-induced ferroelectric phase.

II. EXPERIMENTS

Single crystals of CFGO or CFAO of nominal compositions were prepared by the floating zone technique[23]. The crystals were cut into rectangular shapes with typical dimensions of $0.98 \times 1.34 \times 1.55$ mm^3, in which three axes are along [110], $[1\bar{1}0]$, and [001] directions. Uniaxial pressure p, whose magnitude can be controlled even when the sample is at low temperatures, was applied along the $[1\bar{1}0]$ direction. For details of the uniaxial pressure devices and the pressure cell, see Refs. 24 and 25. In all the experiments in this study, p was always applied at 25 K. The real/imaginary part of dielectric constant, ϵ'/ϵ'' was measured at 10 kHz using the LCR meter (Agilent 4980A), where the electrodes consisted of silver paste painted onto the [110] surfaces. Ferroelectric polarization with the [110] electrodes, $P_{[110]}$, was deduced by the time integration of a polarization current, which was measured with an electrometer (Keithley 6517A). Before the measurements of $P_{[110]}$, a poling electric field $E_{\rm p}$ was applied during the cooling process, and then removed. Neutron-diffraction measurements under applied p were carried out using the two-axis diffractometer E4 installed

at the Berlin Neutron Scattering Center in the Helmholtz Zentrum Berlin for Materials and Energy. The wavelength of the incident neutron was 2.44 Å. Since $p \parallel [1\bar{1}0]$ is applied along the vertical direction, the scattering plane is the (H, H, L) plane.

III. RESULTS

A. $CuFe_{1-x}Ga_xO_2$ (x = 0.035)

1. *p - T phase diagram for Ga 3.5% sample*

Figures 2 (a) – 2 (d) show the temperature dependence of a magnetic wave propagation wave number q, integrated intensities of the (q,q,3/2) and the (1/2-q,1/2-q,3/2) magnetic reflections, $P_{[110]}$, and ϵ', of CFGO with x = 0.035 at ambient pressure, which are consistent with the previous study[13,27]. In the OPD and the FE-ICM phase, q is almost independent of T; and in the PD phase, q depends on T. As shown in Fig. 2(i), below $T_{\rm N2}^{\rm low}$, we can observe (1/2-q,1/2-q,3/2) magnetic Bragg reflections, which originate from the initial phase difference between spins with the helical magnetic ordering in the unit cell[15]. Concomitantly with the magnetic phase transition into the FE-ICM phase, $P_{[110]}$ appears below $T_{\rm N2}^{\rm low}$, and ϵ' shows peaks at $T_{\rm N2}^{\rm low}$. As clearly seen in Figs. 2 (b) and 2 (c), the 1/2-q reflections are good indicators of the FE-ICM phase.

The results of the same measurements under applied p of 400 MPa are shown in Figs. 2 (e) – 2 (h). With decreasing T, q starts to vary at $T_{\rm N2}^{\rm high} \sim 16$ K, which indicates a magnetic phase transition from the OPD phase, although q in the heating process still depends on T. Since $P_{[110]}$ emerges and ϵ' shows a peak at 16 K, ferroelectric transition occurs simultaneously with this magnetic transition. On the other hand, the (1/2-q,1/2-q,3/2) magnetic Bragg reflections can be measured below 9 K even under applied p = 400 MPa. These results clearly indicate that the FE-ICM phase is not realized at 16 K. Therefore, we conclude that applied p induces a new magnetoferroelectric phase. Hereafter, we refer to the p-induced ferroelectric phase as the FE2 phase.

To better understand the p-induced ferroelectric nature of the system, we measured temperature dependence of $P_{[110]}$, ϵ', and ϵ'' under several applied p [Figs. 3(a) – 3(c)]. First, ferroelectricity in the FE2 phase is evidenced by the polarity reversal depending on the sign of $E_{\rm p}$, as shown in the inset in Fig. 3(a). In addition, we have confirmed that a thermally

stimulated current, which originates from residual charges trapped in the sample during the cooling process under applied $E_{\rm p}$[28], does not contribute to $P_{[110]}$ observed under applied p in all the samples investigated here[29]. With increasing p, the absolute value of $P_{[110]}$ at 2 K and the $P_{[110]}$ disappearance temperature drastically increase. The p enhancement of $P_{[110]}$ will be discussed in Sec. III A 2. The $P_{[110]}$ disappearance temperatures correspond to the ϵ peak temperatures on heating under applied p. The peak values in T dependence of ϵ show a maximum at $p \simeq 200$ MPa, and their thermal hysteresis is the greatest at $p \simeq 350$ MPa. In combination with the results of the neutron diffraction experiments[30], we summarize these results as the T-p magnetoelectric phase diagram shown in Fig. 4, where the phase boundary lines determined by the magnetic (dielectric or ferroelectric) measurements are indicated by the blue (red) lines. Hereafter, we refer to the temperature where a phase transition occurs into the FE2 phase as $T_{\rm FE2}$, which is defined by using only the data of $P_{[110]}$ and ϵ. As shown in Fig. 4, $T_{\rm FE2}$ dose not correspond to $T_{\rm N2}^{\rm high}$ in the range of 200 MPa $\leq p \leq$ 350 MPa (also see the supplemental material[30]), while above 350 MPa, a magnetic phase transition from the OPD phase and the ferroelectric transition into the FE2 phase simultaneously occur, namely $T_{\rm FE2} \simeq T_{\rm N2}^{\rm high}$, as mentioned above.

It is worth mentioning here that ϵ (especially during an increasing T process) shows two maxima in the range of 200 MPa $\leq p \leq$ 400 MPa, as shown in Figs. 3 (b) and 3 (c). Correspondingly, $P_{[110]}$ also shows a step like anomaly between 300 MPa $\leq p \leq$ 400 MPa (see also Figs. 2 (g) and 2 (h)). Currently, however, the origin of these anomalies is unclear.

2. Magnetic structure in the FE2 phase

To determine the microscopic origin of $P_{[110]}$ in the FE2 phase, we have performed a tentative magnetic structure analysis in the FE2 phase, following the same procedure outlined in Ref. 14. Figures 5 (a) and 5 (b) show the index L dependence of the experimentally observed "spin orientation factor" ($\rm SOF_{ex}$) of the (q,q,L) and the (1/2-q,1/2-q,L) magnetic reflections at 2 K under applied $p = 400$ MPa and the calculated SOF ($\rm SOF_{cal}$) curves for the proper screw helical ordering[31]. We basically confirmed that the magnetic structure in the FE-ICM phase is the well-studied screw helical one. We compared the L dependence of $\rm SOF_{ex}$ of the (q,q,L) magnetic reflections at 14 K under applied p of 400 MPa with the $\rm SOF_{cal}$ curve for the sinusoidal ordering as realized in the PD phase (Fig. 5 (c)) and that

for the proper screw helical ordering (Fig. 5 (d)). Even by taking into account the rather limited accuracy, the L dependence of SOF_{ex} seem to follow the SOF_{cal} of the sinusoidal magnetic structure, not the helical magnetic one. Therefore, the FE2 phase is shown to be entirely different from the FE-ICM phase also from the viewpoint of the magnetic structure, which suggests that the origin of ferroelectricity is different in both phases. In addition, these results indicate that $P_{[110]}$ originating in the FE2 phase does not contribute to the p enhancement of $P_{[110]}$ at 2 K. As mentioned above, the absolute value of $P_{[110]}$ at 2 K increases with increasing p, and $P_{[110]}$ at 600 MPa is ~ 1200 μC/m^2, which is almost double the value of $P_{[110]}$ at 10 MPa. As shown in Fig. 3(d), the p enhancement of $P_{[110]}$ is a linear extension of the previous study[26], where it is considered to originate from change in the Fe3d-O2p hybridization coupling constants. Note that the $P_{[110]}$ value can be varied by change in the q domain structures originating from the trigonal symmetry around the c axis[24,32]. The application of slight p ($\leq$ 10 MPa), however, results in an almost single q domain structure[26,33]. Therefore, a repopulation of the q domains volume fractions can not cause the $P_{[110]}$ value enhancement.

Note that for the well-known cycloidal structure, which can generate the ferroelectric polarization[3], SOF_{cal} curve is independent of L, or increases with increasing L, if the spiral plane with the magnetic modulation wave vector (q,q,3/2) is within c-(110) plane, or within a-b plane, respectively[15]. Therefore, the magnetic structure in the FE2 phase is not of the cycloidal type.

B. $CuFe_{1-x}Ga_xO_2$ (x = 0.018)

In Figs. 6(a) – 6(o), we show the temperature dependence of q, the integrated intensities of the (q,q,3/2) and the (1/2-q,1/2-q,3/2) magnetic reflections, $P_{[110]}$, ϵ', and ϵ'', of CFGO with x = 0.018 under selected applied p. All of the p = 0 Pa data are consistent with the previous work[25]. Using the same procedure as in the Ga 3.5% sample, we determined the magnetic and ferroelectric phase transitions. We found that as in the Ga 3.5% sample, the application of $p \geq 400$ MPa induces another ferroelectric phase, which is different from the FE-ICM phase, in the temperature region indicated by the red hatching in Figs. 6(f) – 6(o). Tentatively, we refer to the p-induced ferroelectric phase and the $P_{[110]}$ emergence temperature as the FE2 phase and T_{FE2}, respectively, in the same way as for the Ga 3.5%

sample. Hereafter, we describe the p evolution of the magnetic and ferroelectric properties of CFGO with x = 0.018.

As shown in the inset in Figs. 6(c) and 6(d), an additional peak structure in the T dependence of ϵ appears at $\sim$ 200 MPa, while $P_{[110]}$ in the FE2 phase starts to emerge at p = 400 MPa ($T_{\rm FE2} \simeq$ 15.5 K) [Fig. 6(h)]. Remarkably, in contrast to the results for CFGO with x = 0.035, no magnetic anomaly can be seen in the T dependence of q and the integrated intensities at $T_{\rm FE2}$, even under applied p of 600 MPa [Figs. 6(f) – 6(h) and 6(k) – 6(m)], whereas this result seems to be the same as that for the Ga 3.5% sample in the range of 200 MPa $\leq p \leq$ 350 MPa. This result suggests that the ferroelectric transition into the FE2 phase is not accompanied by the magnetic phase transition in CFGO with x = 0.018. It should be noted here that there are the case that the magnetic modulation wave vector in the spin-driven ferroelectric $Mn_{1-x}Co_xWO_4$ shows no change during the phase transitions between collinear magnetic phases (paraelectric) and spiral magnetic phases (ferroelectric)[34,35]. To clarify whether a magnetic phase transition occur at $T_{\rm FE2}$ or not, further precise measurements are needed. We summarize these results as the T-p magnetoelectric phase diagram shown in Fig. 7.

As the temperature dependence of the integrated intensities in Fig. 6 shows, several magnetic orders coexist in the temperature region 8 K $\leq T \leq$ 14 K. Concerning, we make two remarks. First, in the T-p magnetoelectric phase diagram of the Ga 1.8% sample, we have plotted the phase transition temperature into or from the FE-ICM phase, using only the T derivative of ϵ' for the sake of clarity (the blue-hatched regions in Fig. 6 are also based on the same definition). This definition roughly corresponds to the neutron diffraction data, and is especially in good agreement with the 1/2-q reflections in the temperature region 8 K $\leq T \leq$ 10 K. Second, as shown in Figs. 6(f) – 6(g) and 6(k) – 6(l), the (q,q,3/2) reflection labeled FE-ICM appears at 12 $\sim$ 14 K simultaneously with those labeled FE2 under applied $p \geq$ 400 MPa[36]. As can be clearly seen, especially in Figs. 6(i) and 6(j), the coexistence of the FE-ICM and FE2 magnetic orderings result in a rather complex T dependence of ϵ in the temperature region 10 K $\leq T \leq$ 14 K.

As mentioned above, the emergence of $P_{[110]}$ at $T_{\rm FE2}$ may not involve a magnetic phase transition. We emphasize, however, that when the system undergoes a magnetic phase transition into the FE-ICM and the 4SL phases, $P_{[110]}$ decreases and finally disappears, as shown in Fig. 6(m). In other words, the disappearance of the volume fraction of the FE2

magnetic ordering corresponds to that of $P_{[110]}$. Therefore, the magnetic ordering in the FE2 phase must have some relationship with the origin of $P_{[110]}$ in the FE2 phase. Possible models explaining the observed dependencies will be discussed in Sec. IV. Note that although the finite value of $P_{[110]}$ was observed under applied $p = 600$ MPa even in the 4SL phase (see Fig. 6(m)), this originates from the fact that the FE-ICM phase is stabilized under applied p and remains partly present[25]. Furthermore, as in the Ga 3.5% sample, the p enhancement of $P_{[110]}$ in the FE-ICM phase can be seen also in CFGO with x = 0.018, although it is not a linear function of p (not shown) due to the coexistence of several magnetic orderings. Taking into account that $P_{[110]}$ can not be observed in the 4SL phase (except for the FE-ICM component), these results evidence that the p enhancement of $P_{[110]}$ is caused not by the conventional piezoelectric effect due to the lattice displacements, but by change in the microscopic d-p hybridization coupling constants, as claimed in Ref. 26. This discussion must be applicable to the p enhancement of $P_{[110]}$ in the FE-ICM phase of the Ga 3.5% sample.

C. $CuFe_{1-x}Al_xO_2$ (x = 0.050)

Finally, in Figs. 8(a) – 8(e), we show the results of the Al 5% sample, which is expected to have almost the same nature as the Ga 8 % sample[37]. Since the OPD phase is realized down to the lowest temperature at ambient pressure, q is independent of T, and $P_{[110]}$ remains 0 C/m^2 [Figs. 8(a) – 8(c)]. With increasing p, $P_{[110]}$ starts to emerge at $\sim$ 150 MPa [Fig. 8(d)] (we have confirmed the polarity reversal of $P_{[110]}$ depending on the sign of $E_{\rm p}$), and ϵ' in T dependence shows a peak structure at the $P_{[110]}$ disappearance temperature. Hereafter, we expediently refer to the p-induced ferroelectric phase and the $P_{[110]}$ disappearance temperature as the FE2 phase and $T_{\rm FE2}$, respectively, in the same way as for the Ga 3.5% and Ga 1.8% samples. As shown in Figs. 8(a) – 8(c), during the cooling process, q under applied $p \geq 300$MPa begins to vary around $T_{\rm FE2}$, indicating that the ferroelectric transition into the FE2 phase is accompanied by a magnetic phase transition from the OPD phase in CFAO with x = 0.050. As in the Ga 3.5% sample, q in the heating process depends on T. Moreover, the $P_{[110]}$ values are almost saturated by the largest $E_{\rm p} \simeq 217$ kV/m in this experiment [Fig. 8(e)]. Compared with the sensitivity of $P_{[110]}$ to $E_{\rm p}$ in the FE-ICM phase[38], $P_{[110]}$ in the FE2 phase seems to be more sensitive to $E_{\rm p}$. We summarize these results as

the T-p magnetoelectric phase diagram shown in Fig. 9(a).

As in the Ga 3.5% sample, we compared the L dependence of $\mathrm{SOF_{ex}}$ of the (q,q,L) magnetic reflections in the FE2 phase ($T = 2$ K, $p = 600$ MPa) with the $\mathrm{SOF_{cal}}$ curves (the (1/2-q,1/2-q,L) magnetic reflections were not observed), as shown in Fig. 9(b). As a result, the magnetic structure in the FE2 phase of the Al 5% sample is also expected to be of the sinusoidal type, which certainly indicates that the p-induced phase is not the FE-ICM phase. Note that as mentioned in Sec. I, the sinusoidal ordering in the OPD phase is oblique from the c axis, which was deduced from the magnetic Bragg reflections beyond the (H,H,L) zone by using a four-circle neutron diffractometer[14]. However, diffraction measurements restricted to the (H,H,L) zone can not determine the extent of the difference in tilt between the PD and the OPD magnetic orderings, and thus cannot distinguish these orderings[39].

IV. DISCUSSION

Let us consider the origin of the ferroelectricity in the FE2 phase. In the FE-ICM phase, the proper screw helical magnetic structure itself breaks the inversion symmetry in the system, which results in the induction of ferroelectric polarization through the d-p hybridization mechanism. On the other hand, the sinusoidal magnetic ordering in the FE2 phase does not itself break the inversion symmetry in the system, because it preserves the the mirror plane perpendicular to the [110] axis. Therefore, when we take only the magnetic structure in the FE2 phase into account, the ferroelectricity in the FE2 phase can be considered not to be the spin-driven type, and thus an additional lattice displacement induced by applied p accounts for $P_{[110]}$ in the FE2 phase as conventional ferroelectrics. However, we suggest that the magnetic ordering in the FE2 phase has some relation to the origin of ferroelectricity, taking into account that (i) the FE2 phase is magnetically distinguishable from the OPD or the FE-ICM phases, as displayed in the Ga 3.5%, Al 5.0% samples, and (ii) the suggestive results shown in the Ga 1.8% sample: the disappearance of the volume fraction of the FE2 magnetic ordering corresponds to that of $P_{[110]}$, as emphasized in Sec.III B.

Here, carefully looking at the three phase diagrams (Figs. 4, 7, and 9(a)), we find that the FE2 phase boundary lines with no magnetic anomalies are always present in the part adjacent to the PD phase. In fact, the magnetic structure in the FE2 phase seems to be

of the sinusoidal type as in the PD phase [see Figs. 5 and 9(b)]. This indicates that from the magnetic viewpoint, the FE2 phase is hardly distinguishable from the PD phase within this experimental accuracy. Therefore, one possible explanation is that there are some tiny modifications of the sinusoidal magnetic structure, which are induced by applied p through the spin-lattice coupling in this system, and they result in the inversion symmetry breaking and the emergence of $P_{[110]}$ in the FE2 phase.

Another feasible origin of the ferroelectricity in the FE2 phase could be that the application of p induces further slight lattice distortions coupled with the sinusoidal magnetic structure through the spin-lattice coupling, where the inversion symmetry is broken not by the magnetic structure, but by further slight lattice distortions. From this explanation, however, it follows that after the system enters the polar lattice phase (the FE2 phase), the system reenters the nonpolar lattice phases (the FE-ICM or 4SL phases) "by spontaneously further distorting". To test this rather surprising consequence, a synchrotron radiation x-ray diffraction study under applied p is highly desirable.

We have proposed the two feasible origins of the ferroelectricity in the FE2 phase, in both of which the spin-lattice coupling in this system plays a crucial role. Our tentative magnetic structure analysis is, however, restricted to the (H,H,L) plane, and thus there remains the possibility that the magnetic structure in the FE2 phase is of a noncollinear type that breaks the inversion symmetry. Moreover, although we have expediently referred to the p-induced ferroelectric phase in all the samples investigated here as the FE2 phase, there remains a possibility that these phases are different from each other. It is therefore of a primary importance to perform a more detail magnetic structure analysis in the p-induced ferroelectric phase using magnetic reflections in the wider reciprocal lattice space beyond the (H,H,L) plane.

V. SUMMARY AND CONCLUSION

We have systematically investigated the magnetic and ferroelectric properties of CFGO with x = 0.035, 0.018 and CFAO with x = 0.050 under applied p along the $[1\bar{1}0]$ direction up to 600 MPa. We have found that the application of p induces a new ferroelectric phase (FE2 phase), which is different from the well-studied FE-ICM phase, in all the samples investigated in this current study. From the T dependence of q under applied p, the FE2

phase is magnetically distinguishable from the OPD or the FE-ICM phases, while it cannot be magnetically distinguished from the PD phase and, in fact, the magnetic structure in the FE2 phase seems to be of the collinear sinusoidal type, as in the PD phase. Although the sinusoidal magnetic ordering does not break the inversion symmetry itself, our experimental results suggest that it plays an important role in the origin of the ferroelectricity in the FE2 phase through the spin-lattice coupling. Based on these results, we propose two possible origins of the ferroelectricity in the FE2 phase: (i) the application of p induces some tiny modifications from the sinusoidal magnetic structure through the spin-lattice coupling in this system, and this modified magnetic structure results in the inversion symmetry breaking and the emergence of $P_{[110]}$ in the FE2 phase; or (ii) further slight lattice distortions by applied p, which is coupled with the sinusoidal magnetic orderings through the spin-lattice coupling, breaks the inversion symmetry and yields $P_{[110]}$. To categorically confirm the origin of the ferroelectricity in the FE2 phase, a more detail magnetic structure analysis and a synchrotron radiation x-ray diffraction study under applied p are needed. This study demonstrates that the uniaxial pressure is one of powerful external controllable parameters for investigation of spin-driven ferroelectric materials with spin-lattice coupling.

ACKNOWLEDGMENTS

We thank HZB for the allocation of neutron beamtime. The neutron diffraction experiments at HZB were carried out according to Proposal Nos. 14100387-ST and 16103652-ST, which were transferred from HQR(T1-1) installed at JRR-3 with the approval of Institute for Solid State Physics, The University of Tokyo (Proposal Nos. NSL-00000329 and NSL-00000519), Japan Atomic Energy Agency, Tokai, Japan. This work was supported by a Grant-in-Aid for Scientific Research (C) (Grant Nos. 23540424 and 26400369) from Japan Society for the Promotion of Science.

---

* E-mail address: tamatsukuri@nsmsmac4.ph.kagu.tus.ac.jp

† Present address: RIKEN Center for Emergent Matter Science (CEMS), Saitama 351-0198, Japan

[1] T. Kimura, T. Goto, H. Shintani, K. Ishizaka, T. Arima, and Y. Tokura, Nature (London) **426**, 55 (2003).

[2] W. Eerenstein, N. D. Mathur, and J. F. Scott, Nature (London) **442**, 759 (2006).

[3] Y. Tokura, S. Seki, and N. Nagaosa, Rep. Prog. Phys. **77**, 076501 (2014).

[4] T. Kimura and Y. Tokura, J. Phys.: Condens. Matter **20**, 434204 (2008).

[5] T. Arima, J. Phys. Soc. Jpn. **80**, 052001 (2011).

[6] Y. Yamashita and K. Ueda, Phys. Rev. Lett. **85**, 4960 (2000).

[7] F. Becca and F. Mila, Phys. Rev. Lett. **89**, 037204 (2002).

[8] D. L. Bergman, R. Shindou, G. A. Fiete, and L. Balents, Phys. Rev. B **74**, 134409 (2006).

[9] F. Wang and A. Vishwanath, Phys. Rev. Lett. **100**, 077201 (2008).

[10] M. Mekata, N. Yaguchi, T. Takagi, T. Sugino, S. Mitsuda, H. Yoshizawa, N. Hosoito, and T. Shinjo, J. Phys. Soc. Jpn. **62**, 4474 (1993).

[11] S. Mitsuda, N. Kasahara, T. Uno, and M. Mase, J. Phys. Soc. Jpn. **67**, 4026 (1998).

[12] N. Terada, T. Nakajima, S. Mitsuda, and H. Kitazawa, J. Phys. Conf. Ser. **145**, 012071 (2009).

[13] N. Terada, T. Nakajima, S. Mitsuda, H. Kitazawa, K. Kaneko, and N. Metoki, Phys. Rev. B **78**, 014101 (2008).

[14] N. Terada, T. Kawasaki, S. Mitsuda, H. Kimura, and Y. Noda, J. Phys. Soc. Jpn. **74**, 1561 (2005).

[15] T. Nakajima, S. Mitsuda, S. Kanetsuki, K. Prokes, A. Podlesnyak, H. Kimura, and Y. Noda, J. Phys. Soc. Jpn. **76**, 043709 (2007).

[16] T. Nakajima, S. Mitsuda, S. Kanetsuki, K. Tanaka, K. Fujii, N. Terada, M. Soda, M. Matsuura, and K. Hirota, Phys. Rev. B **77**, 052401 (2008).

[17] T. Arima, J. Phys. Soc. Jpn. **76**, 073702 (2007).

[18] F. Ye, Y. Ren, Q. Huang, J. A. Fernandez-Baca, P. Dai, J. W. Lynn, and T. Kimura, Phys. Rev. B **73**, 220404(R) (2006).

[19] N. Terada, S. Mitsuda, H. Ohsumi, and K. Tajima, J. Phys. Soc. Jpn. **75**, 023602 (2006).

[20] G. Quirion, M. J. Tagore, M. L. Plumer, and O. A. Petrenko, Phys. Rev. B **77**, 094111 (2008).

[21] T. Nakajima, S. Mitsuda, T. Inami, N. Terada, H. Ohsumi, K. Prokes, and A. Podlesnyak, Phys. Rev. B **78**, 024106 (2008).

[22] H. Tamatsukuri, S. Aoki, S. Mitsuda, T. Nakajima, T. Nakamura, T. Itabashi, S. Hosaka, S. Ito, Y. Yamasaki, H. Nakao, K. Prokes, and K. Kiefer, Phys. Rev. B **94**, 174402 (2016).

[23] T. R. Zhao, M. Hasegawa, and H. Takei, J. Cryst. Growth **166**, 408 (1996).

[24] T. Nakajima, S. Mitsuda, T. Nakamura, H. Ishii, T. Haku, Y. Honma, M. Kosaka, N. Aso, and Y. Uwatoko, Phys. Rev. B **83**, 220101 (2011).

[25] T. Nakajima, S. Mitsuda, K. Takahashi, K. Yoshitomi, K. Masuda, C. Kaneko, Y. Honma, S. Kobayashi, H. Kitazawa, M. Kosaka, N. Aso, Y. Uwatoko, N. Terada, S. Wakimoto, M. Takeda, and K. Kakurai, J. Phys. Soc. Jpn. **81**, 094710 (2012).

[26] S. Mitsuda, K. Yoshitomi, T. Nakajima, C. Kaneko, H. Yamazaki, M. Kosaka, N. Aso, Y. Uwatoko, Y. Noda, M. Matsuura, N. Terada, S. Wakimoto, M. Takeda, and K. Kakurai, J. Phys.: Conf. Ser. **340**, 012062 (2012).

[27] We could not distinguish magnetic reflections of each magnetic orders in the intermediate T regions due to a limited resolution compared with the previous study[13], and thus we analyzed the data using the single gaussian function. In addition, $T_{\rm N2}^{\rm high} \simeq 13.5$ K in this study (see Fig. 2(a) and 2(b)) is rather high compared with the previous works ($\sim$10 K), which may come from the smaller, 3.5 %, concentration of Ga^{3+} ions than expected.

[28] T. Nakajima, S. Mitsuda, H. Yamazaki, and M. Matsuura, J. Phys. Soc. Jpn. **82**, 024706 (2013).

[29] To check this point, we have monitored the time dependence of the current for 30 minutes at a fixed temperature during the $P_{[110]}$ measurements in the heating process, and have observed no current. If the thermally stimulated current contributes to the current, a current flow having temperature dependent relaxation time must be observed. On the other hand, "pure" pyroelectric current must not be observed during the 30 minutes, because $P_{[110]}$ at the fixed temperature does not change.

[30] In the Supplemental Material at [URL will be inserted by publisher], we describe the phase transition temperature and the phase boundary from the OPD phase to the PD or FE2 phases in the intermediate region (200 MPa $\leq p \leq$ 350 MPa).

[31] Because the attenuation and absorption by the pressure cell was not corrected in this experiment, the accuracy of the integrated intensity is limited. However, the magnetic structure in the well-studied FE-ICM phase is almost consistent with the helical one. This fact guarantees our discussion described in the main text.

[32] H. Tamatsukuri, S. Mitsuda, T. Nakajima, K. Shibata, C. Kaneko, K. Takehana, Y. Imanaka, N. Terada, H. Kitazawa, K. Prokes, S. Matas, K. Kiefer, S. Paeckel, A. Sokolowski, B. Klemke, and S. Gerischer, Phys. Rev. B **93**, 174101 (2016).

[33] T. Nakajima, S. Mitsuda, T. Haku, K. Shibata, K. Yoshitomi, Y. Noda, N. Aso, Y. Uwatoko, and N. Terada, J. Phys. Soc. Jpn. **80**, 014714 (2011).

[34] G. Lautenschläger, H. Weitzel, T. Vogt, R. Hock, A. Böhm, M. Bonnet, and H. Fuess, Phys. Rev. B **48**, 6087 (1993).

[35] F. Ye, S. Chi, J. A. Fernandez-Baca, H. Cao, K.-C. Liang, Y. Wang, B. Lorenz, and C. W. Chu, Phys. Rev. B **86**, 094429 (2012).

[36] In the Supplemental Material at [URL will be inserted by publisher], we show typical neutron diffraction profiles and the fitting results of the Ga 1.8% sample under applied p of 400 MPa at selected temperature.

[37] We have confirmed that the bulk properties of the Ga 8.0% sample under applied p are almost the same as those of the Al 5.0% sample (not shown).

[38] T. Nakajima, S. Mitsuda, K. Takahashi, M. Yamano, K. Masuda, H. Yamazaki, K. Prokes, K. Kiefer, S. Gerischer, N. Terada, H. Kitazawa, M. Matsuda, K. Kakurai, H. Kimura, Y. Noda, M. Soda, M. Matsuura, and K. Hirota, Phys. Rev. B **79**, 214423 (2009).

[39] Moreover, the detail magnetic structure analysis shown in Ref. 14 deduced that the sinusoidal ordering is oblique from the c axis by $\sim 18^\circ$ even in the PD phase. This fact presents us further difficulties in determining the extent of the difference in tilt between the PD and the OPD ordering.

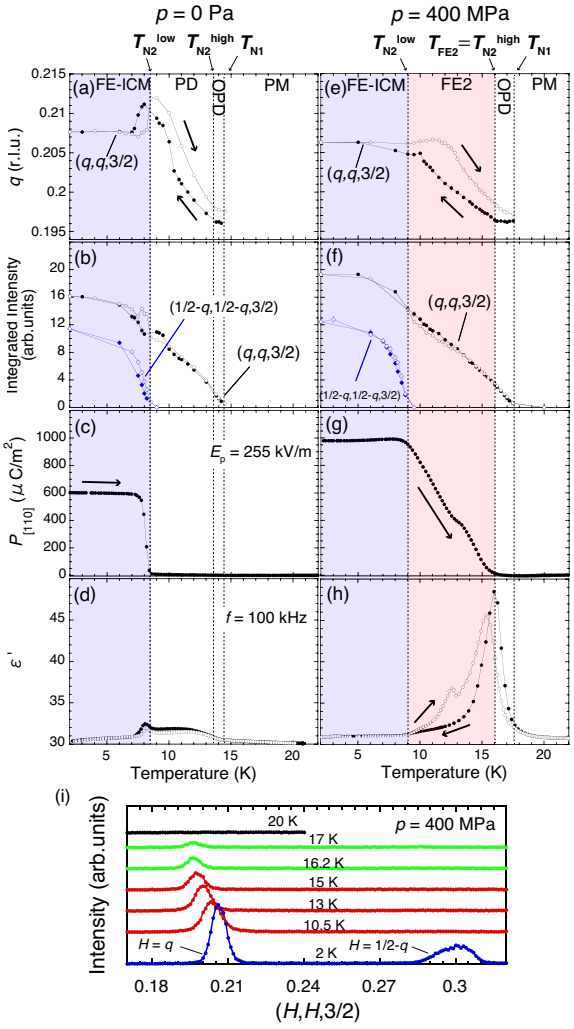

FIG. 2. (Color Online) Temperature dependence of magnetic propagation wave number q, integrated intensities of $(q,q,3/2)$ and $(1/2\text{-}q,1/2\text{-}q,3/2)$ magnetic reflections, $P_{[110]}$, and ϵ' of $CuFe_{1-x}Ga_xO_2$ with x = 0.035 at ambient pressure [(a)-(d)] and under 400 MPa [(e)-(h)], respectively. Open and closed symbols denote data measured with increasing and decreasing temperature, respectively, except for $P_{[110]}$ data ($P_{[110]}$ were measured on a heating run). Note that the data of $P_{[110]}$ and ϵ' for $p = 0$ Pa were measured under slightly applied p ($\leq$ 10 MPa) in order to produce the single q domain state (see Sec. III A 2 in the main text). The application of slight p, however, does not affect the magnetic phase transition temperatures. (i) Typical neutron diffraction profiles at selected temperature under applied p of 400 MPa. The overall features of the $p = 0$ Pa data are the same as those of the $p = 400$ MPa data.

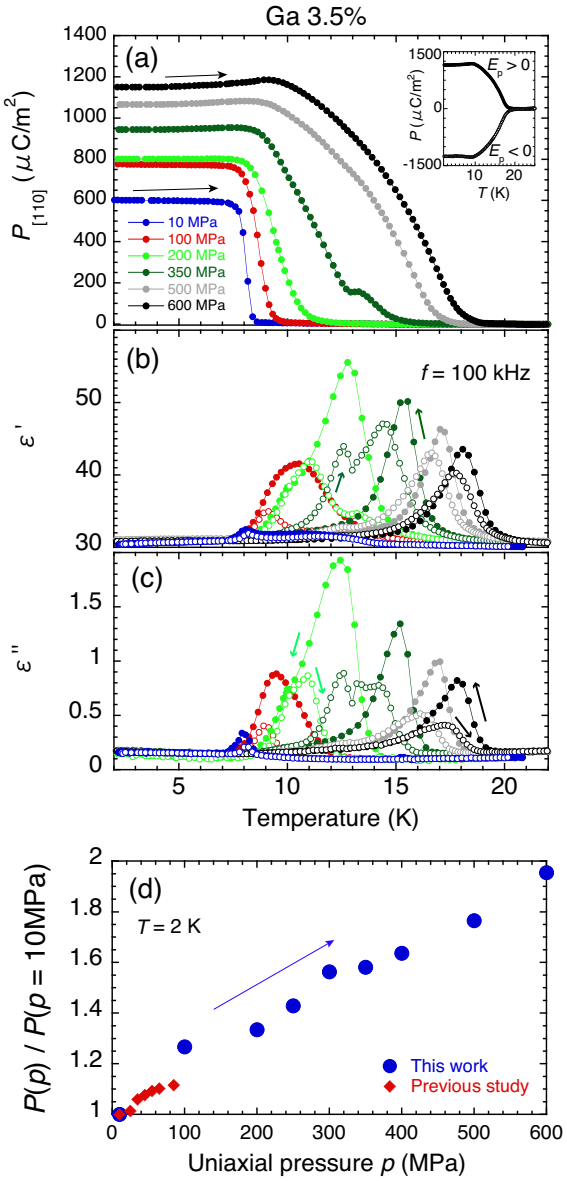

FIG. 3. (Color Online) Temperature dependence of (a) $P_{[110]}$, (b) ϵ', and (c) ϵ'' under selected applied p. The inset shows $E_{\rm p}$ sign dependence of $P_{[110]}$ under applied p of 600 MPa ($|E_{\rm p}|$ = 255 kV/m). (d) Electric polarization enhancement factor at 2 K as a function of applied p. Data shown by red diamonds are redrawn from Ref. 26.

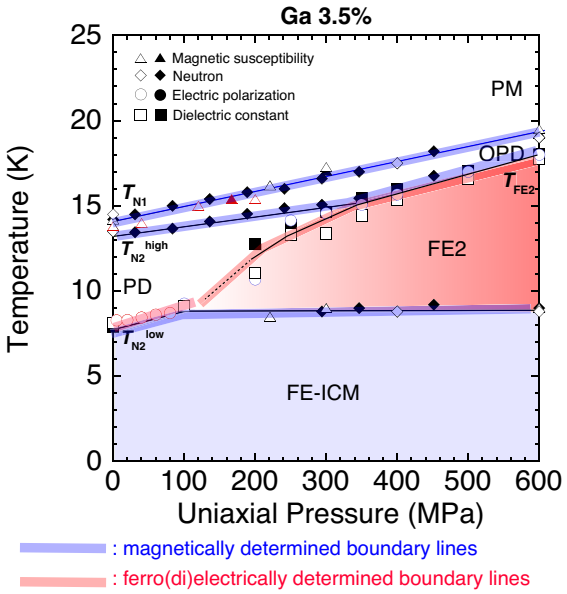

FIG. 4. (Color Online) Temperature vs. uniaxial pressure ($\parallel (1\bar{1}0)$) magnetic phase diagram of CFGO (x = 0.035). Open and closed symbols denote data measured with increasing and decreasing temperature, respectively.

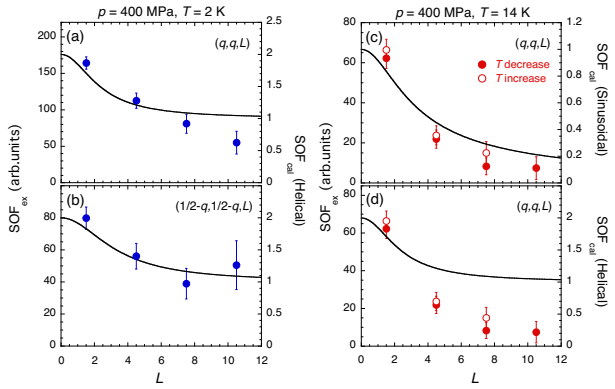

FIG. 5. (Color Online) L dependence of experimentally observed spin orientation factor ($\mathrm{SOF_{ex}}$) of (a) the (q,q,3/2) and (b) the (1/2-q,1/2-q,3/2) magnetic reflections at 2 K under applied $p = 400$ MPa, and calculated spin orientation factor ($\mathrm{SOF_{cal}}$) curves for the proper screw helical ordering. L dependence of $\mathrm{SOF_{ex}}$ of the (q,q,3/2) magnetic reflections at 14 K under applied $p = 400$ MPa with a $\mathrm{SOF_{cal}}$ curve (c) for the sinusoidal ordering and (d) for the proper screw helical ordering.

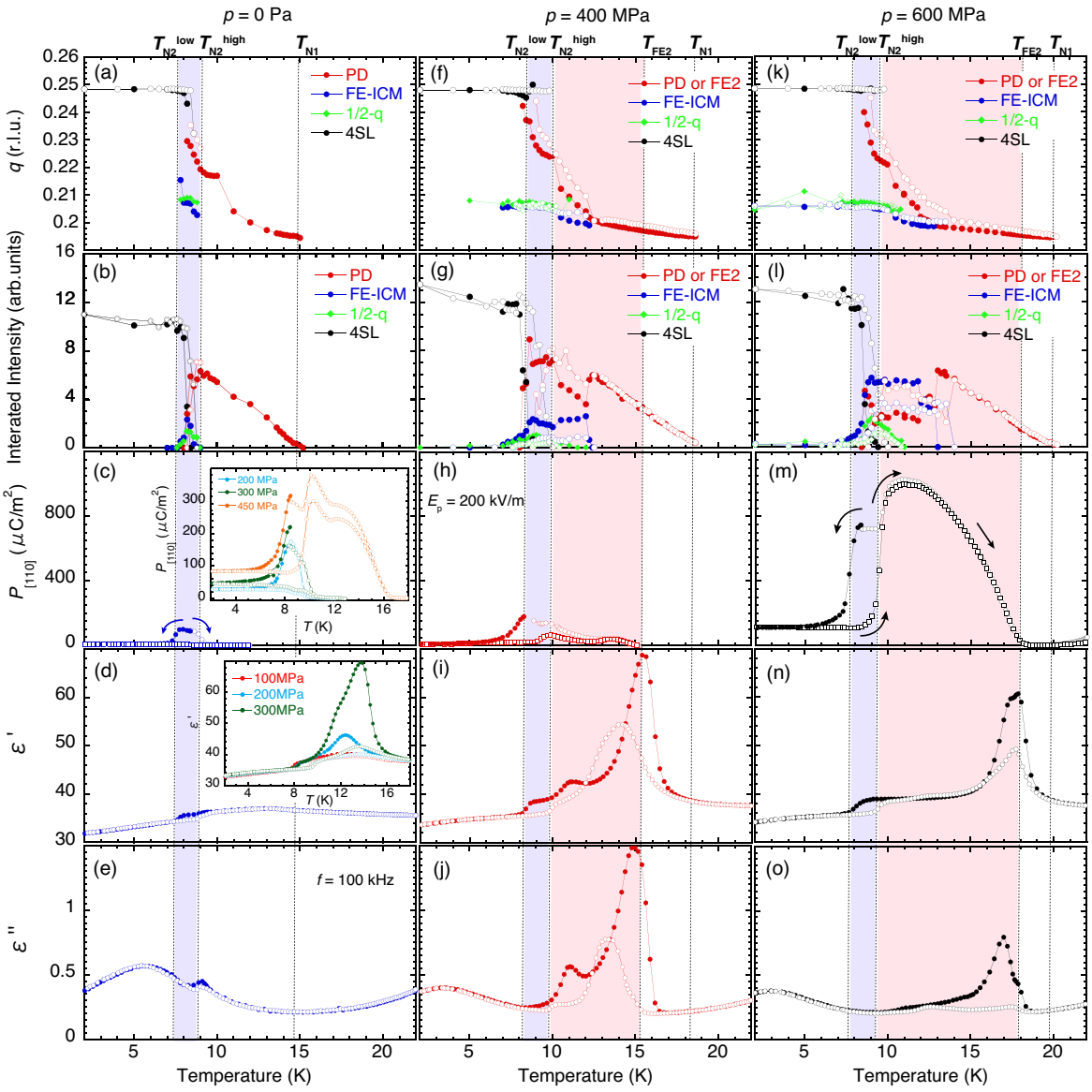

FIG. 6. (Color Online) Temperature dependence of q, integrated intensities of the (q,q,3/2) and (1/2-q,1/2-q,3/2) magnetic reflections, $P_{[110]}$, ϵ', ϵ'' of $CuFe_{1-x}Ga_xO_2$ with x = 0.018 at ambient pressure [(a)-(e)], and under applied p of 400 MPa [(f)-(j)], and 600 MPa [(k)-(o)], respectively. Open and closed symbols denote data measured with increasing and decreasing temperature, respectively.

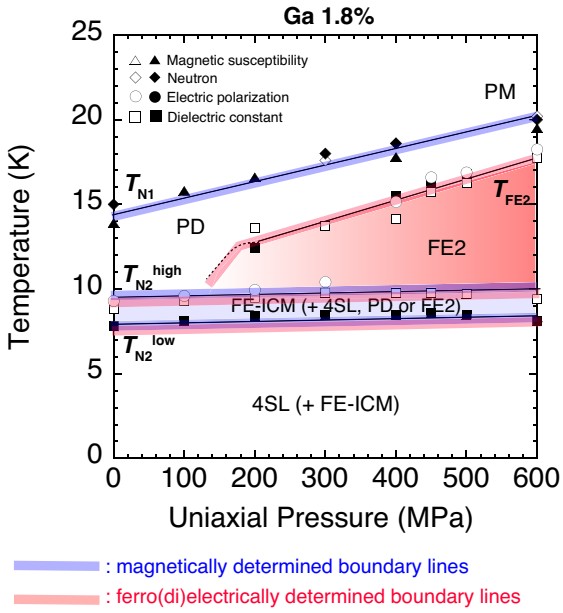

FIG. 7. (Color Online) Temperature vs. uniaxial pressure ($\parallel (1\bar{1}0)$) magnetic phase diagram of CFGO (x=0.018). Open and closed symbols denote data measured with increasing and decreasing temperature, respectively.

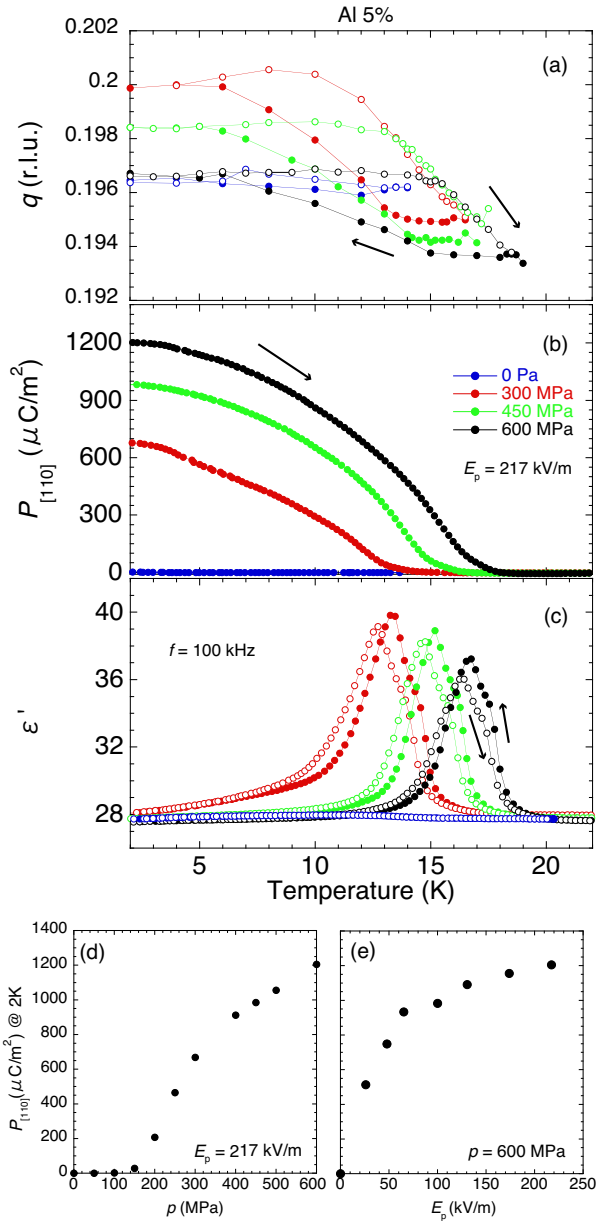

FIG. 8. (Color Online) Temperature dependence of (a) q, (b) $P_{[110]}$, and (c) ϵ' under selected applied p. Open and closed symbols denote data measured with increasing and decreasing temperature, respectively, except for the $P_{[110]}$ data. (d) p dependence of $P_{[110]}$ at 2 K. (e) $E_{\rm p}$ dependence of $P_{[110]}$ at 2 K under applied p of 600 MPa.

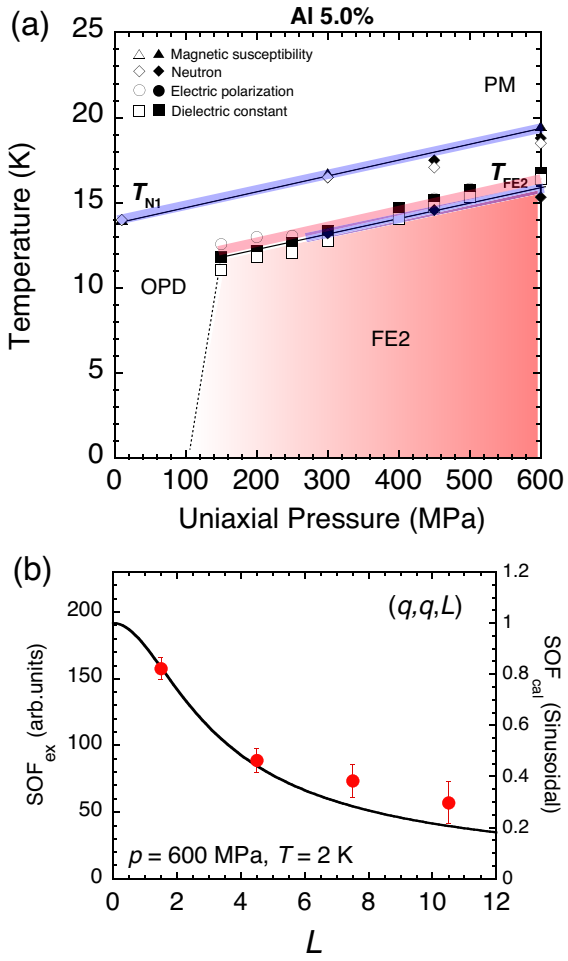

FIG. 9. (Color Online) (a) Temperature vs. uniaxial pressure ($\parallel (1\bar{1}0)$) magnetic phase diagram of CFAO (x = 0.050). Open and closed symbols denote data measured with increasing and decreasing temperature, respectively. (b) L dependence of $\mathrm{SOF_{ex}}$ of the (q,q,3/2) magnetic reflections at 2 K under applied p = 600 MPa, and $\mathrm{SOF_{cal}}$ curves for sinusoidal ordering.